J Seismol (2019) 23:801–818
https://doi.org/10.1007/s10950-019-09835-0

ORIGINAL ARTICLE

# Another look at the 2009 seismic activity, Harrat Lunayyir, Saudi Arabia

**Ali K. Abdelfattah · Salvatore de Lorenzo · S. Almadani · M. Fnais · H. Alfaifi · N. Al-Arifi**

Received: 1 March 2018 / Accepted: 10 May 2019 / Published online: 29 May 2019


**Abstract** This study aims to recognize the influence of source- and path-effects on seismic spectra using the waveform data from the 2009 seismic activity, Harrat Lunayyir (HL), eastern flank of the Red Sea coastline, Saudi Arabia. This seismic activity is considered as a series of continuously evolving events reaching at some stage the maximum on 19 May 2009, with the largest shock of Mw 5.4, and then decayed. A total number of 218 events of magnitudes $M_L \geq 2.0$ were analyzed, which include the largest shock, 101 and 116 seismic events representing the seismic events within the early and decay stages, respectively. The data analysis using Frequency-time analysis revealed diversity patterns of frequency contents along the recorded seismic stations. Moreover, the modified WADATI diagram showed $V_P/V_S$ variations of $1.7 \pm 0.003$ and $1.72 \pm 0.002$ before and after the occurrence of the largest-sized event among the HL seismic activity, respectively. Using the grid-search method to recover the space parameters representing the average source spectrum of each earthquake over the recorded seismic stations, estimates of source sizes and stress drops imply variations in self-similarity scaling relationship among the HL seismic activity. According to the results obtained from the current analyses, we propose a scenario began with an emplacement of seismic activity due to the local stress accumulation imports from an upward dike injection that is blocked by cooled and hardened magmatic materials in the upper crust from the earlier intrusions. The stress accumulation continued and was then released, at some stage, by the event having the maximum magnitude followed by seismic activities released due to stress relaxations.

**Keywords** Spectral characteristics · $V_P/V_S$ ratio · Source parameters · Tectonic and sequence activity · Saudi Arabia

A. K. Abdelfattah (✉) · S. Almadani · M. Fnais · H. Alfaifi · N. Al-Arifi
Department of Geology & Geophysics, King Saud University, Riyadh 11451, Kingdom of Saudi Arabia
e-mail: ali_kamel100@yahoo.co.uk

S. de Lorenzo
Dipartimento di Scienze della Terra, University di Bari "Aldo Moro", Via Orabona 4, I-70125 Bari, Italy

## 1 Introduction

The Arabian shield that lies to the east of the Red Sea rift is characterized by a wide distribution of ancient Cenozoic basaltic fields where local seismic activities occurred. Owing to this geodynamic process, many earthquakes recently occurred in the shield. These earthquakes include the 2009 Harrat Lunayyir (HL) earthquake of Mw 4.8 (Abdelfattah et al. 2014) and the 2009 Badr earthquake of Mw 3.7 (Aldamegh et al. 2010), in the northwestern part of the shield. These earthquakes revealed the presence of normal faulting in the NNW-SSE striking plane. Recently, the 2014 Jizan earthquake of Mw 4.4 along the eastern Red Sea coastline, near the Yemen-KSA border, occurred. The focal mechanism solution shows dextral strike-slip faulting along the ENE-WSW striking plane (Abdelfattah et al. 2017).

The generation mechanism of an earthquake sequence is potentially influenced by the heterogeneous distribution of stress regime, heat flow, and fracture strength on a fault zone. On the other hand, earthquakes of tectonic origin are frequently observed along the continental margins following the rift systems characterized by stress releases and are different from the earthquakes which occur due to dike intrusions or volcanic eruptions (Pedersen et al. 2007; Ibs-von Seht et al. 2008; Kiratzi et al. 2008).

The analysis of source characteristics of the HL earthquake sequence is considered as a promising study that can help us to understand the enigmatic phenomena of the peculiar seismicity processes in the Arabian shield. In this study, we used the high-quality waveform data for earthquakes of magnitudes $M_L \geq 2.0$ to characterize any distinctive variations in frequency content, averaged $V_P/V_S$ ratio, and stress drop in order to elucidate generation processes among the 2009 HL seismic activity. The results were interpreted in terms of the present day geodynamic processes.

### 1.1 Tectonic setting

Owing to the geodynamic processes, the tectonic-magmatic activities are presumably coupled in the Arabian Shield (El-Isa and Shanti 1989; Daradich et al. 2003; Pallister et al. 2010; Hansen et al. 2013). Volcanism initiated during the late Miocene in the Arabian Shield and the last eruption occurred ~ 759 AD (Camp et al. 1987). In the epicenter area, the plutonic rocks of diorite to tonalite compositions carry imprints of several cycles of metamorphism and tectonism through Tertiary–Quaternary age are present (Al-Amri and Fnais 2009). Along the northern part of the Arabian shield, the NE-SW extension stress is manifested by a number of NW-SE normal Cenozoic fault trends that are subparallel to the rifting system of the Red Sea (Brown 1972; Mukhopadhyay et al. 2012). Moreover, a number of dikes (Johnson 2006) and volcanic cones that formed over Precambrian crystalline rocks are oriented along the NNW trend.

Based on the focal mechanism solutions and hypocenter distributions, the normal faults of NNW strike are suggested to be ruptured during the 2009 earthquake sequence associated with dyke intrusions (Baer and Hamiel 2010; Pallister et al. 2010; Craig et al. 2011; Mukhopadhyay et al. 2012; Hansen et al. 2013). The crustal deformation model based on InSAR data indicates that the 2009 earthquake sequence was accompanied by the intrusion of a dike spanning 10 km, having a strike of 340° (Baer and Hamiel 2010) that may be related to the dominantly low-frequency events. Owing to the release of aseismic slip along the dike opening, estimates of the seismic moment and geodetic (seismic and aseismic) moment showed a ratio of 6% and 14%, as determined by Pallister et al. (2010) and Baer and Hamiel (2010), respectively. A similar ratio of 4% and 10% was observed for the 2004 and 2005 Dallol intrusions, Afar region (Wright et al. 2006; Grandin et al. 2009; Nobile et al. 2012).

The crustal deformation associated with the HL seismic activity was modeled by a vertical-dike intrusion with a NNW-SSE strike direction (Baer and Hamiel 2010; Pallister et al. 2010). An incipient status of dike intrusion was also suggested by Mukhopadhyay et al. (2012). The respective sequence was classified as mixed-frequency events containing both high-frequency and very low-frequency contents (Pallister et al. 2010). A seismic tomography study (Hansen et al. 2013) revealed that magmatic intrusions of fast velocity were obliquely extended upwards to the NNW trend. Recently, seismic tomography models of Sychev et al. (2017), Koulakov et al. (2015), and Koulakov et al. (2014) speculated mechanisms of gas emission and fluid propagation in the area. Moreover, Zobin et al. (2013) suggested two scenarios showing that the volcanic eruption at HL is less likely to occur; in that, the sub-surface intrusion was arrested or the dike was injected along the rift zones. The source parameters of the largest events retrieved by Abdelfattah et al. (2014) exhibited high stress-release earthquakes associated with low seismic wave attenuation that characterizes the upper crust of the Arabian Shield, indicating that potential intraplate earthquakes are riskier than interplate ones.

### 1.2 Data and seismicity

In the present study, we used the digital waveform data of the events from a moderate-sized earthquake sequence of Mw 4.8 (Abdelfattah et al. 2014) that occurred in HL, northwest the Arabian Shield, Saudi Arabia, on the 19th of May 2009 approximately 60 km east of the Red Sea margin. We used the waveform recordings of the nearby seismic network that was installed by the Saudi Geological Survey (SGS) and King Abdulaziz City of Science and Technology (KACST) soon after the earthquake sequence started in April 2009. It comprises twenty-two

three-component stations. Each station is equipped with Trillium broadband velocity sensors characterized by a response range of 0.02 to 120 s, digitizer of 100 sample/s, and 142 dB dynamic range of the whole recording system. The distribution and the high number of broadband seismic observations installed in the epicenter area, immediately after the earthquake sequence started in April 2009, gave an impetus in order to understand whether the tectonic or magmatic processes produced the HL seismic activity. The temporary seismic network improved the station coverage over the epicenter area. The dataset is composed of the recordings of a total number of 218 events of magnitudes $M_L \geq 2.0$; they were used to investigate the spectral characteristics of the HL activity. The waveforms were manually filtered to avoid any recording problems such as noise, missed recordings, overlapping of successive earthquakes, or early cutoff of well-developed waves. The selected events appropriately cover the sequence activity in space and time distributions. Figure 1 shows a schematic map of the main tectonic features in the region, the station distribution, and the epicenters of the events having magnitudes greater than zero.

Many multidisciplinary studies have been carried out on HL and its seismicity using the data of the 2009 earthquake sequence. The focal mechanism of the largest shock computed by Craig et al. (2011) using waveform inversion shows a normal faulting mechanism of two nodal planes striking along NNW-SSE orientation, reflecting a dominant NE extensional tectonic regime. For the seismic events released before the largest shock, the hypocenter relocations that were refined by Abdelfattah et al. (2017) showed the alignment of epicenters distributed along the western edge of the seismic activity and delineated a NNW-SSE trend parallel to the Red Sea (Fig. 2). Moreover, in the episode of the decay activity, the seismic activity at the eastern edge zone shows two clusters of shallower and deeper focal depths. Hansen et al. (2013) found out that the early stage activity was created by upward movement of the magmatic dike intrusion, oriented along the NNW-SSE direction, while the decay stage activity was related to local stress redistributions triggered by the intrusion.

### 1.3 Time-frequency analysis

Spectral characteristics of earthquake sources located nearby or within magma chambers and dikes provide insights into geodynamic processes and rock fracture processes, as well as the physical properties of rocks and fluids between the sources and the receivers (Chouet 1996; Dawson and Chouet 2014; McNutt 2005). Seismograms recorded by seismic stations above or near the magma chambers are characterized by impulsive transients to long-lasting tremors (McNutt 2005; Neuberg et al. 2006; Tuffen and Dingwell 2005). A number of studies showed that volcanic earthquakes and tremors are triggered by magmatic or geothermal activities. The spectral characteristics of volcanic earthquakes and tremors are quite different from those of tectonic earthquakes.

The spectral characteristics of seismic signals can reflect important insights about the dynamics of fracture processes and the rock properties between source and receiver. However, it is important to separate source from path-effects. To recognize the influence of source and path on seismic signals that characterize the seismic events among the respective sequence, we used the frequency-time analysis (FTAN), as a qualitative technique, to monitor any distinctive features in the spectral characteristics. We investigated the spectral characteristics of seismic signals by following the time-frequency analysis procedure of Levshin et al. (1972) used in surface wave dispersion analyses. This technique is used to discriminate between earthquakes and explosions (Duda and Xu 1988; Duda and Kaiser 1989; Domański 2007), to calculate dispersion curves of surface waves (Levshin et al. 1972), to identify seismic phases and to infer details on earthquake faulting processes (Wilde-Piorko et al. 2011). The nfilter algorithm of Saul (1995), depending on the Hilbert Transform technique, was used in the present analysis.

We investigated the frequency contents among the HL seismic activity for events of magnitude $M_L \geq 2.0$. Because the LNYS station recorded almost all the events of hypocenter distances smaller than 17 km, the waveform data recorded by this station were used in order to classify events having a different frequency content. The different spectral content of the events of the sequence causes different patterns of energy distribution as a function of both time and frequency, as shown in Fig. 3a–c. The spectral characteristics classified the events into three groups of different frequency contents. The high-frequency events (10–30 Hz). The other two groups were identified as mixed-frequency events, one of them characterized the events having two frequency bands in the ranges of 1–10 and 10–30 Hz,

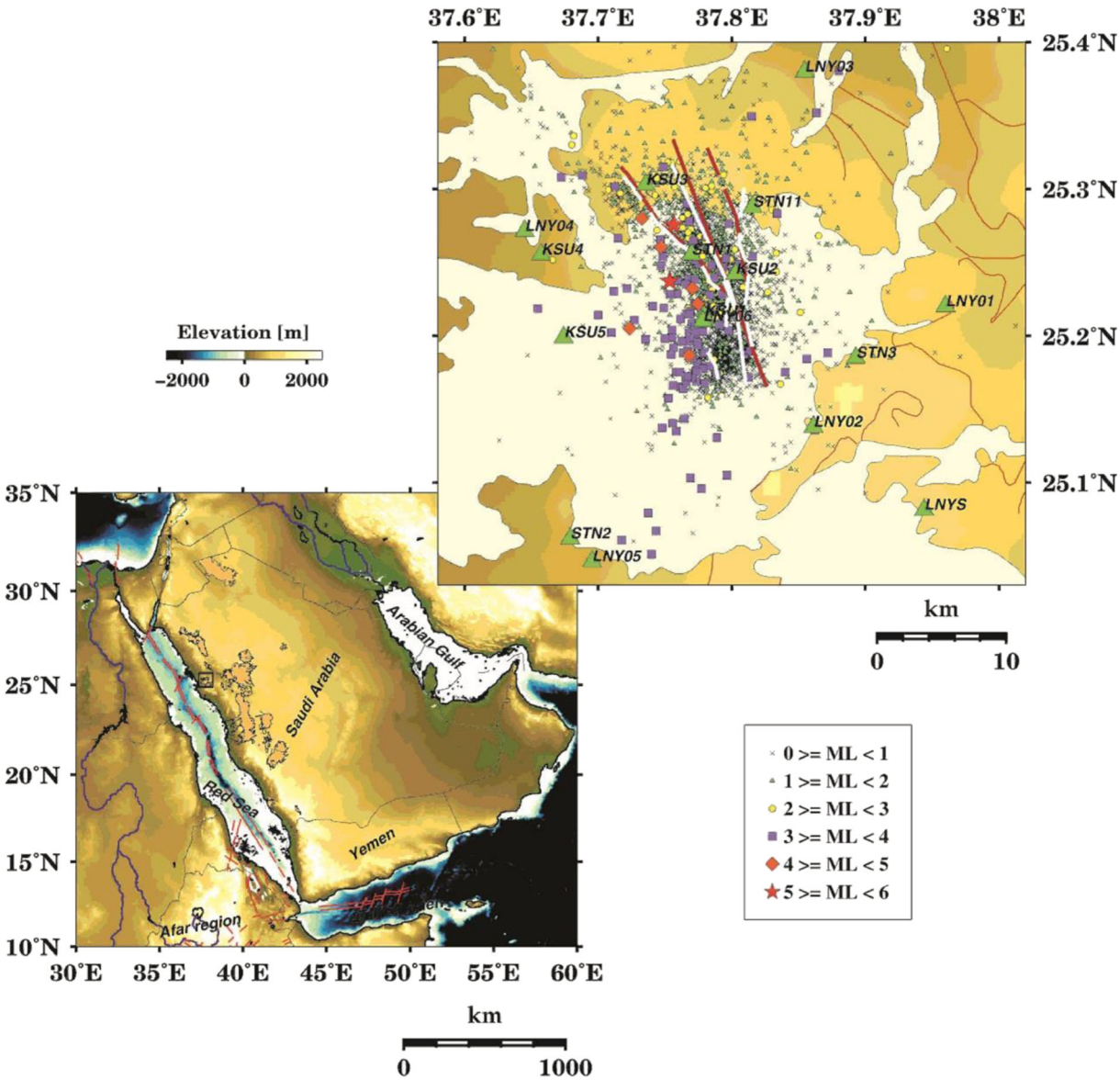


**Fig. 1** The map shows the tectonic plate boundary in the vicinity of the studied area that stands by an open rectangular in the left panel. The spatial distribution of epicenters in the study area is also shown for the 2009 earthquake sequence

and other events exhibited three successive patterns of frequency contents around 0.1–1, 1–10, and 10–30 Hz, implying different source processes. Considering the migration of hypocenters at the early stage of the seismic activity, the patterns that characterized by high-frequency content may correspond to local tectonic processes emplaced by dike intrusion, while the events of a significant low-frequency content may be related to stress relaxations (Fig. 3a–c). Moreover, the path directions to the LNYS station, as shown in Fig. 3d, suggest that the path effects may contribute to some extent the dissimilar patterns in frequency content characteristics.

### 1.4 $V_P/V_S$ ratio

The arrival times of P and S waves were manually picked from the velocity seismograms recorded by the local seismic network shown in Fig. 1. Figure 4 shows an example of the arrival times picked for the event that occurred in 2009/07/04 18:18:13.31 (UTC) of local

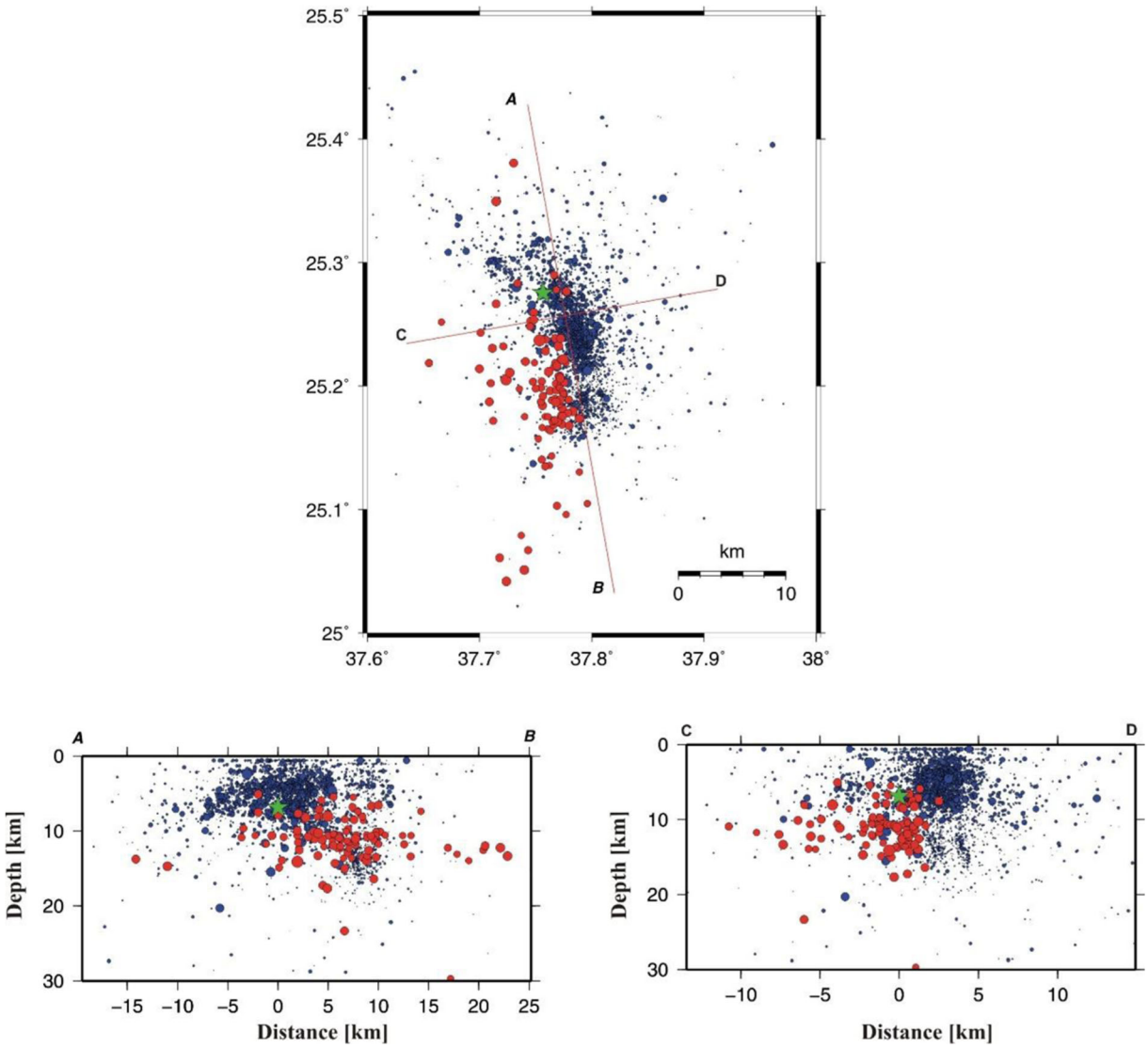


**Fig. 2** The plot shows the spatial distribution of epicenters and hypocenters as a function of magnitudes for the early stage activity (red circles), largest magnitude event (green stars), and the decay stage activity (blue circles)

magnitude 4.2. The data set consists of 2570 P and S phases associated with 218 earthquakes of magnitude ML ≥ 2.0 of good signal-to-noise ratios. The arrival times of events, using the aforementioned criteria were used to calculate the average $V_P/V_S$ ratio using a modified WADATI method (Chatelain 1978). We followed the procedure explained by Maggi et al. (2009) that is based on the differential travel times between phase readings of S waves, $\Delta T_S$, and P waves, $\Delta T_P$, at pair stations. The time differences between the P and S waves at a pair of corresponding stations can be written in the form of;

$$\Delta T_P = |P_i - P_j| = \frac{|x_i - x_j|}{V_P} \tag{1}$$

and

$$\Delta T_S = |S_i - S_j| = \frac{|x_i - x_j|}{V_S} \tag{2}$$

where $x_i$ and $x_j$ are the hypocenter distances of a pair of stations. The arrival times of P and S waves are given by $P_i$, $P_j$, $S_i$, and $S_j$. $V_P$ and $V_S$ are the P and S wave velocities, respectively. Dividing 2 by 1, we obtain:

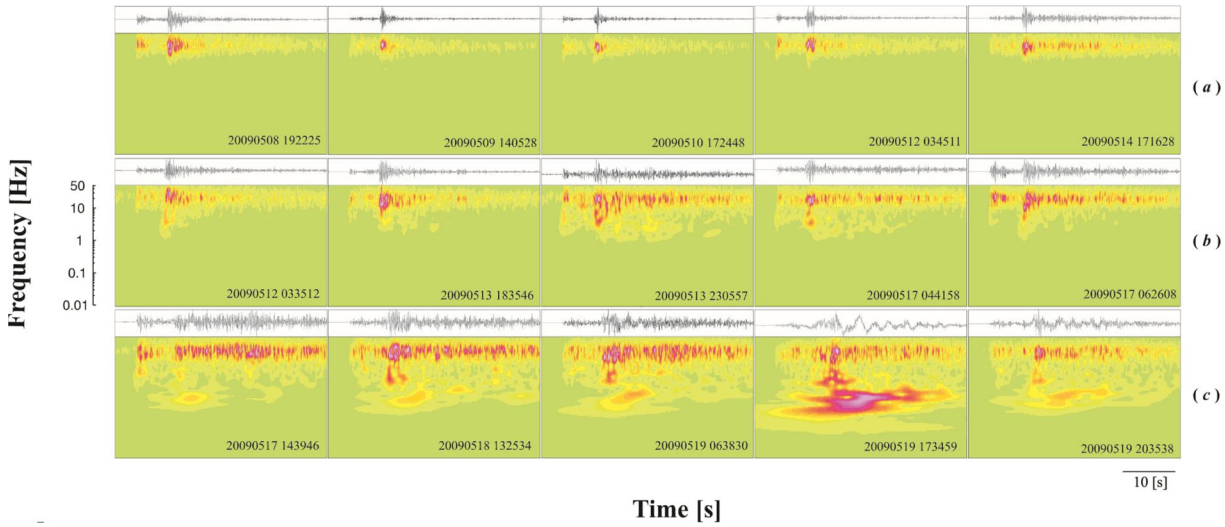


**Fig. 3** gives some examples of the time-frequency analysis. The calculated spectrograms are divided into three groups: **a** the events (red circles) with only high-frequency content (10–30 Hz) that represent the southern cluster of deeper events, were initially released due to the local tectonic process of the dike intrusion, **b** events (green circles) with two frequency bands (1–10 and 10–30 Hz) that represent intermediate events, and **c** events (blue circles) with significant low-frequency content that represent the shallower events in the area of the largest magnitude event. The date and origin time of each seismogram are written below each spectrogram. **d** shows the epicenter and hypocenter distributions of selected earthquakes and location of LNYS seismic station (solid triangles)

$$\frac{\Delta T_S}{\Delta T_P} = \frac{V_P}{V_S} \tag{3}$$

The slope of the straight line that best fits *ΔTs* versus *ΔTp* data for all available earthquakes furnishes an estimate of the $V_P/V_S$ ratio. The Gaussian-Jordan elimination method was used to recover the averaged $V_P/V_S$ ratio. The analysis of the Wadati diagram, using the whole dataset for distances ranging from 0 to 120 km, reveals no significant variations in $V_P/V_S$ ratio before and after the HL largest shock. Alternatively, using the readings of Pg and Sg phases only within hypocenter distances smaller than 38 km, the analysis reveals distinctive variations in the $V_P/V_S$ ratio. Distinctive variations were remarkable for small and typical $V_P/V_S$ ratios of $1.7 \pm 0.003$ and $1.72 \pm 0.002$ that characterized the events in the early and decay stages before and after the largest event, respectively, as shown in Fig. 5. Based on the theory, a linear relation is predicted as long as the $V_P/V_S$ is averaged and constant over the travel path, showing much less sensitive to the $V_P/V_S$ variations. Even if this assumption is invalided, the Wadati diagram is used to resolve an average $V_P/V_S$ beneath seismic network (Kisslinger and Engdahl 1973). The determination of $V_P/V_S$ inferred from the present analysis shows small variations similar to that obtained by Ukawa and Fukao (1981), Chatterjee et al. (1985), Ripepe et al. (2000), Londoño (2010), Lopes and Assumpcão (2011), Gritto and Jarpe (2014), Giannopoulos et al. (2015), and Kaviris et al. (2018). It is noteworthy that most events used in this analysis are located in the upper crust where the velocity zone revealed a moderate $V_P/V_S$ ratio of 1.7 as determined from three-dimensional tomography by Koulakov et al. (2015). Meanwhile, all ray paths traveled upwards into the upper crust at take-off angles greater than 95°, showing a low resolution over the focal zone deeper than 10 km approximately where the $V_P/V_S$ anomaly of 1.8 in the lower crust was obtained by Koulakov et al. (2015).

In the lower panel of Fig. 5, we used the difference in both the travel times and the hypocenter distances between station pairs to determine the apparent velocity of P and S waves. The early stage activity reveals apparent velocities of 6.3 km/s and 3.7 km/s for P and S waves, respectively. During the decay stage, the apparent velocities of P and S waves were 6.7 km/s and 3.9 km/s, respectively.

### 1.5 Source parameters

The P and S waveforms of the events, which were recorded by the largest number of stations and reserved

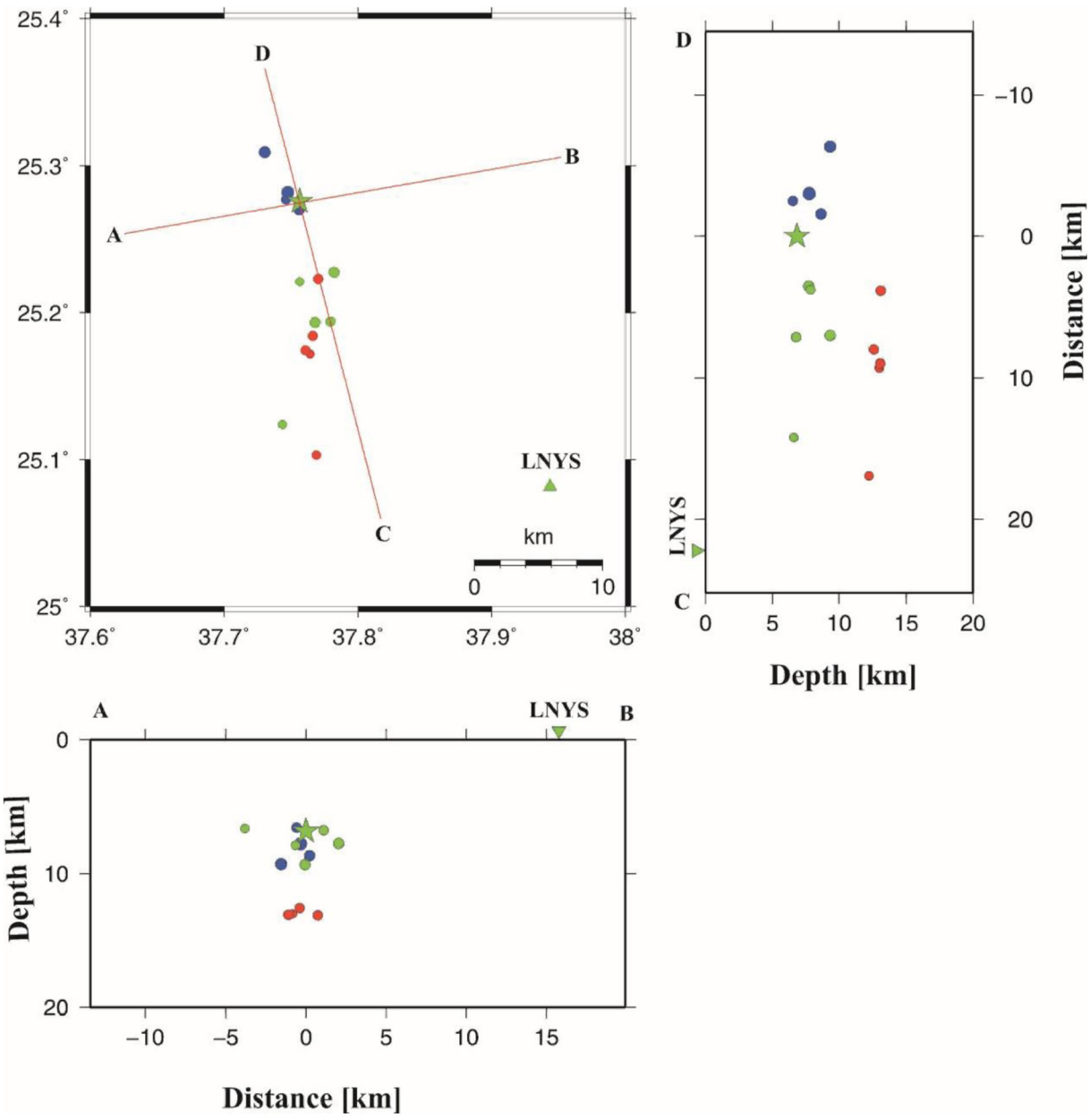


(d)

**Fig. 3** continued.

good signal-to-noise ratio, were used to estimate the source parameters. Before estimating the amplitude spectrum, the recordings were corrected to zero baselines in the time domain. Time windows of 0.6 to 1.2 s lengths that corresponded to 64 and 128 samples starting from the onsets of P and S waves, respectively, were used to compute the Fourier spectrum. To remove the long period biases, a second-order high-pass Butterworth filter of 0.5 Hz corner frequency was applied. In the frequency domain, the average of the three components was carried out to obtain the average amplitude spectrum. The amplitude spectrum was corrected for the instrumental response function and the geometrical spreading factor. We followed the

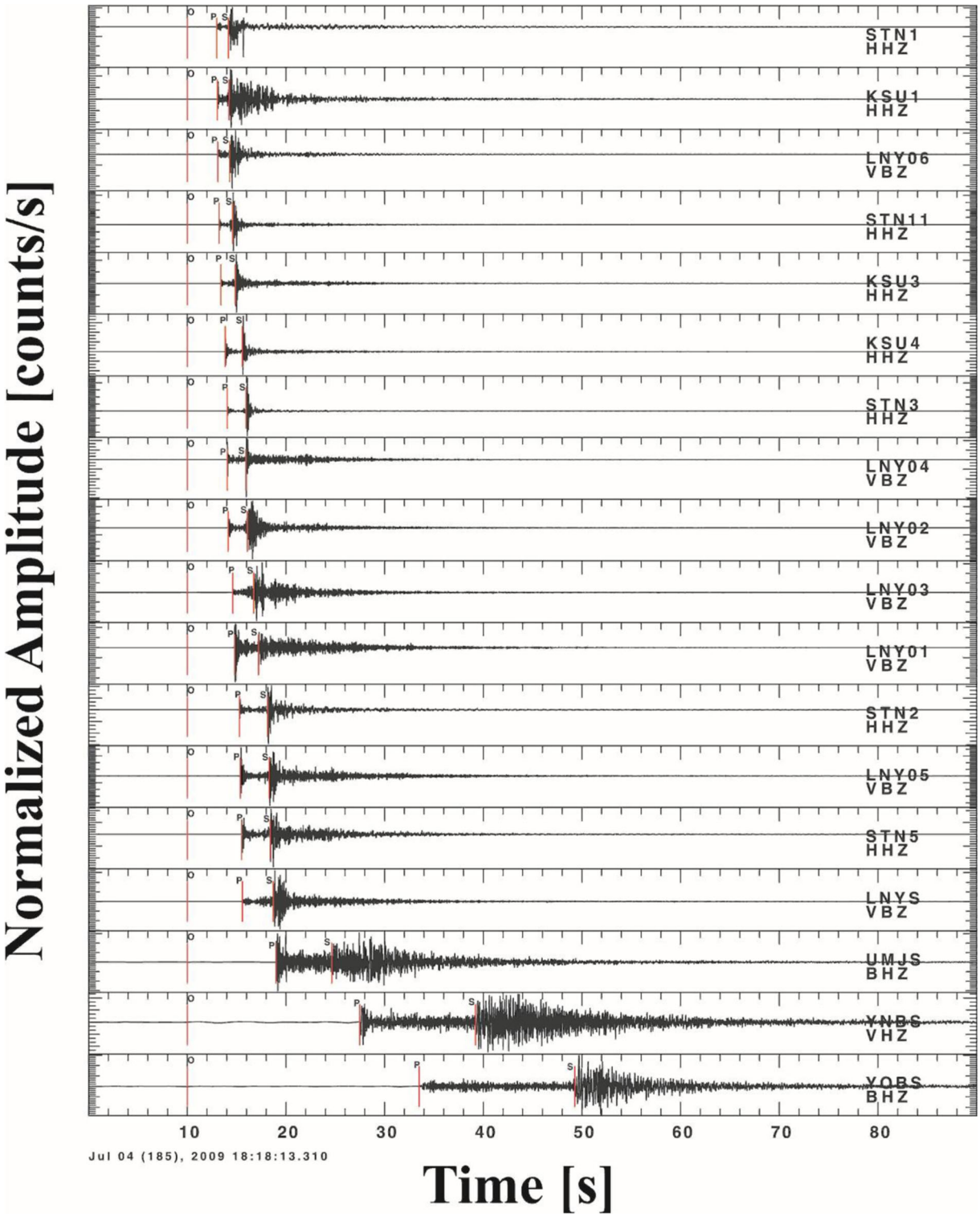


**Fig. 4** Vertical component (velocity) seismograms for the earthquake occurred on 2009/07/04 18:18:13.31 (UTC) $M_L$4.2. Traces were aligned with respect to the origin time (o). Station codes are shown at the right end of each trace. Arrival times of P wave (P) and S wave (S) as identified from the manual picking are also shown

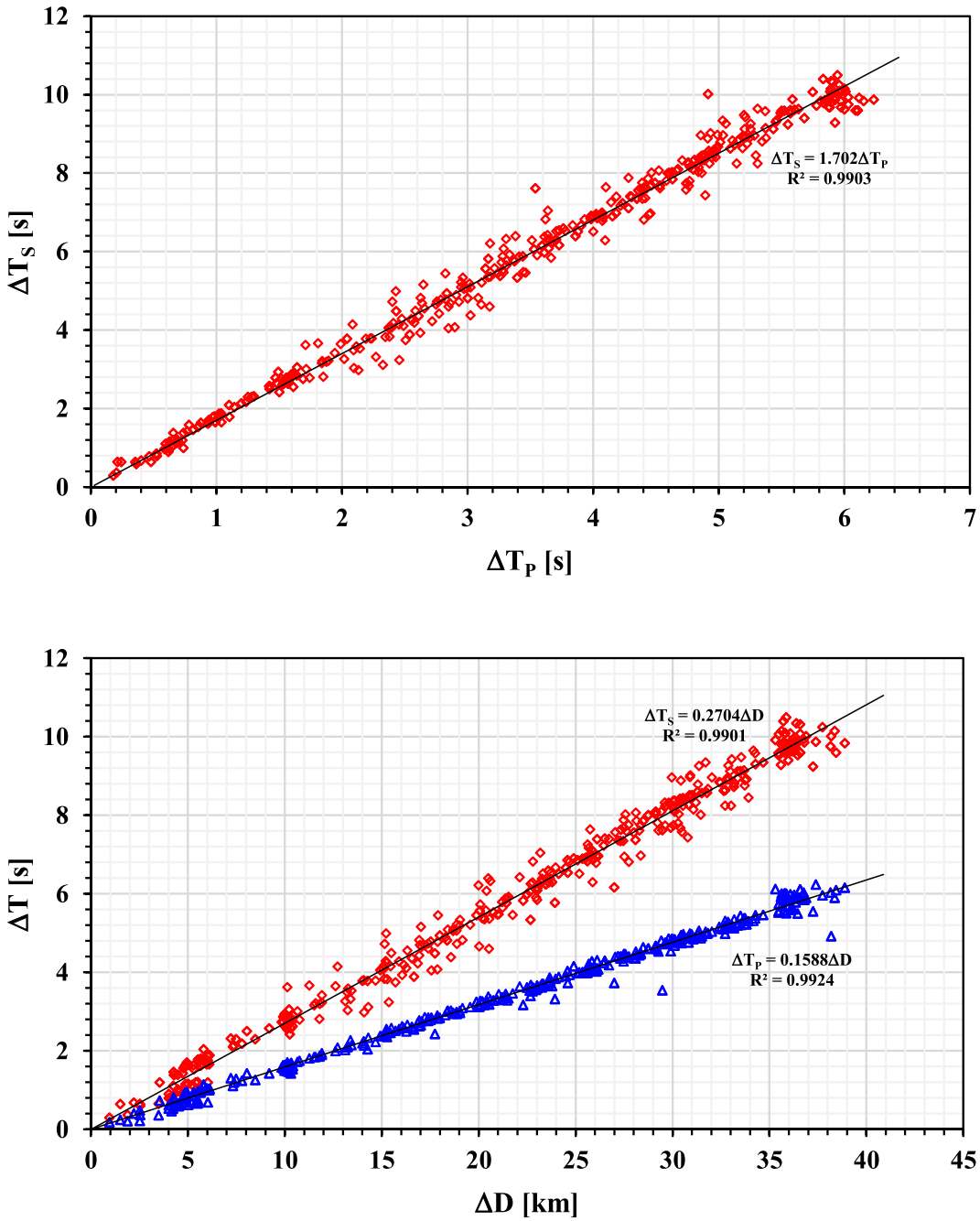


(*a*)

**Fig. 5** The plot showing the relation between the difference in travel times measured between P and S arrival times of station pairs and the corresponding difference in hypocenter distances (ΔD) for **a** the early stage activity and **b** the decay stage activity. The linear least squares method was used to fit the data; obtaining velocities of 6.3–6.7 km/s and 3.7–3.9 km/s for $V_P$ and $V_S$, respectively. The upper panels showed WADATI diagrams that were represented with average $V_P/V_S$ ratios of 1.7 ± 0.003 and 1.72 ± 0.002 for the early stage and the decay stage seismic activities, respectively, with linear correlation coefficients of 0.99

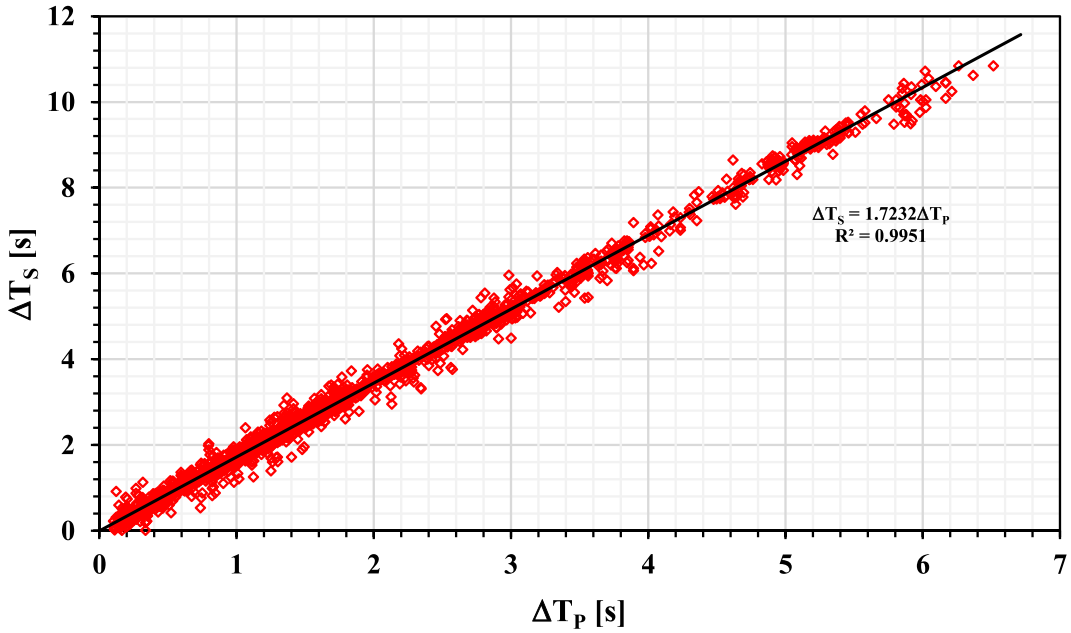


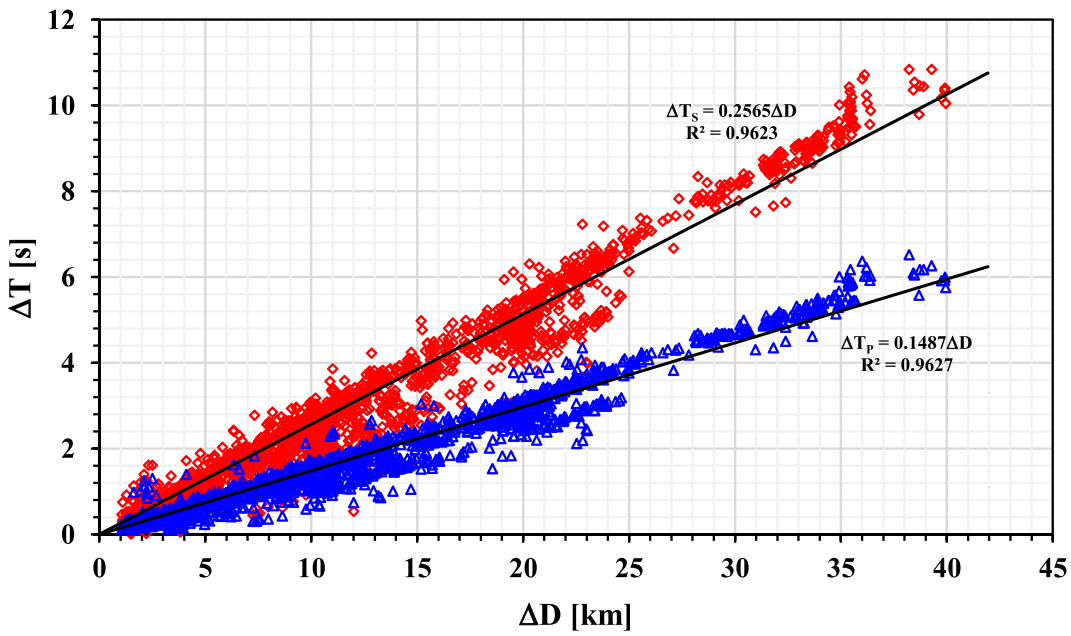


(*b*)

**Fig. 5** continued.

method of Prieto et al. (2004) to correct the path effects from the recorded amplitude spectra by the assumption of the travel path terms between a given cluster and a given station are similar. By analyzing the waveforms in the frequency domain, the source parameters were estimated for the largest event and a total number of 101 and 84 events for the episodes of the HL seismic activity before and after the largest event. We modeled

the Fourier amplitude spectrum using the analytical model of Brune (1970, 1971) that represents the source characteristic parameters in the form of:

$$S(f) = \frac{\Omega_o}{\sqrt{\left(1 + \left(\frac{f}{f_c}\right)^2\right)}} \quad (4)$$

where $\Omega_o$ represents the low-frequency spectral level and $f_c$ the corner frequency. These spectrum characteristic parameters, $\Omega_o$ and $f_c$, were modeled using a grid-search fitting method (e.g., de Lorenzo et al. 2010). Estimates of ($\Omega_o$) and ($f_c$) allow to estimate the seismic moments ($M_o$) using the relationship (Borok 1959);

$$M_o = 4\pi\rho v_P^3 R \frac{\Omega_o}{FR_{\theta\varphi}} \quad (5)$$

where ($\rho$) is the density of 2.7 g/cm$^3$ in the source medium beneath the epicenter area, ($v_P$) is the average P wave velocity in the crust (we used 6.5 as suggested by Rodgers et al. (1999), R is the hypocenter distance from the source-to-receiver, F is the effect of a ground free surface correction that is assumed to double the amplitude for P wave, and the coefficient ($R_{\theta\phi}$) that describes the mean radiation pattern is given to be 0.52 (Aki and Richards 1980).

We used the formula of Hanks and Wyss (1972) to estimate the source radius r:

$$r = \frac{2.34 v_P}{2\pi f_c} \quad (6)$$

The static stress drop ($\Delta\sigma$) was calculated using the seismic moment and source radius relationship of Eshelby (1957) for a circular rupture mode;

$$\Delta\sigma = \frac{7M_o}{16r^3} \quad (7)$$

Figure 6 shows an example of P and S average spectra and the theoretical best fit model for an earthquake recorded at different stations. The calculated seismic moments range between 1.12E + 12 Nm and 1.36E + 17 Nm; the fault radii range approximately between 84 and 1664 m; the stress drops ranges from about 0.6 and 22.3 MPa. To determine the scaling relationship, the calculated seismic moments were plotted vs. the source radius together with lines of constant stress drop range (Fig. 7). The scaling relationship exhibits a clear tendency of deviation from a constant stress drop scaling over the aforementioned magnitude range (Fig. 7). However, a growing trend is observed between the source dimension and the corresponding seismic moment. The trend of the seismic moment against the corner frequency is approximately represented by two segments (Figure 8) represented by $f_o \propto M_o^{-3.1}$ and $f_o \propto M_o^{-5.8}$, respectively, which reveal a significant departure of the decay stage activity from a constant stress drop model. Figure 9 shows the spatial distributions of seismic moments and stress drops among the HL seismic activity.

## 2 Discussion

The present study provides interesting observations that can improve our understanding of the geodynamic processes for local dislocation source zones located in the vicinity of an active rift system. The dataset consisting of 218 earthquakes ($M_L \geq 2.0$) was analyzed in order to find distinctive characteristics among the events of the 2009 earthquake sequence in HL, Saudi Arabia. In the present study, three characteristics have been investigated on the basis of the spatial and temporal distribution of hypocenters; spectral characteristics, $V_P/V_S$ ratios, and stress drop estimates. The earthquakes of similar locations and source mechanisms produce waveform similarities along the same source-to-receiver paths. Seismicity sequences in the flank of the continental rift presumably occur due to the coupling of local stress concentrations caused by the ambient tectonic stress weakening the crust. The highly heterogeneous elastic structure around the hypocenter zone may be the cause of different source characteristics of the same earthquake sequence. The suggestion of Baer and Hamiel (2010), Pallister et al. (2010), and Mukhopadhyay et al. (2012), that attributed the swarm activity to dike intrusions, is consistent with a high-stress drop but it is hard to conciliate with the presence of dominant low-frequency events.

It is worth stressing that most tectonic earthquakes in the Arabian Shield are originated in the upper crust. The hypocenter distributions of seismic events reveal that the seismic events of larger magnitudes among the respective sequence were initially released at a depth of 18 km and then migrated upward gradually in a NNW orientation; according to a dike intrusion reaching shallow depth (Abdelfattah et al. 2017). The seismic activities, that represented the decay stage, are distributed at

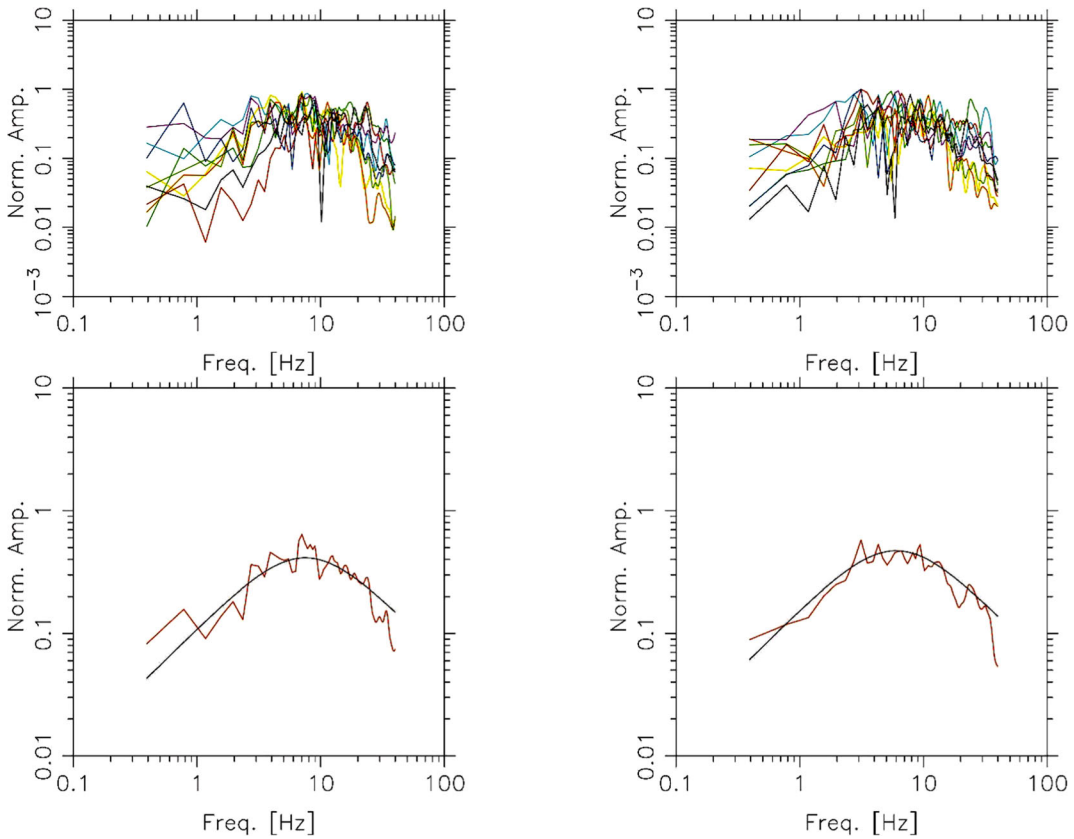


**Fig. 6** An example of amplitude spectrum calculated at each station (the upper panels) and the average amplitude spectrum calculated over the stations (the lower panels). The left and right panels represented P and S waves, respectively

different focal depths within the upper crust; revealing two volumes with 2–8 km and 12–18 km focal depths separated by seismic activities emplaced by a dike intrusion, in the early stage, which moved up and stopped at the largest event location. In the early stage, the epicenters migrated from southeast to northwest, showing activities along the NNW-SSE orientation, parallel to the axial rifting of the Red Sea. This is an important result that provides information on the principal axis of the stress field that produces normal faulting mechanisms in the region. Most of the fault plane solutions previously studied revealed that the sequence activity was characterized by normal faulting mechanisms. The largest shock reflected source mechanism of normal faulting as obtained by Craig et al. (2011). One reverse, two strike-slip, and six normal faulting mechanisms were reported by Hansen et al. (2013). The normal and strike-slip faulting mechanisms are expected to be observed as controlled by the ambient extensional and shear stress regimes transferred into the region from the Red Sea rifting system and Aqaba-Dead Sea Fault system. The normal focal mechanisms strongly emphasize that the seismicity was related to dike intrusions, systematically orientated in the direction of the regional greatest principal stress, consistent with the model introduced by Hill (1977).

The analysis of dataset reveals three typical types of signals with different partitions between high- and low-frequency contents. We propose that the first group of events that characterized by only high-frequency contents may relate to local tectonic process due to a dike intrusion. We found that the second and third group of events having mixed frequency contents may correspond to another process due to stress relaxation with the possible involvement of fluids. Since all seismic stations are located at a unique hard rock, the low-frequency characteristics at some stations are related to travel path effects. The mixed frequency (MF) seismograms and those with very low frequencies were recently observed at Augustine Volcano in Alaska (Pallister et al. 2010). Moreover, the low-frequency component of MF events was suggested by Cramer

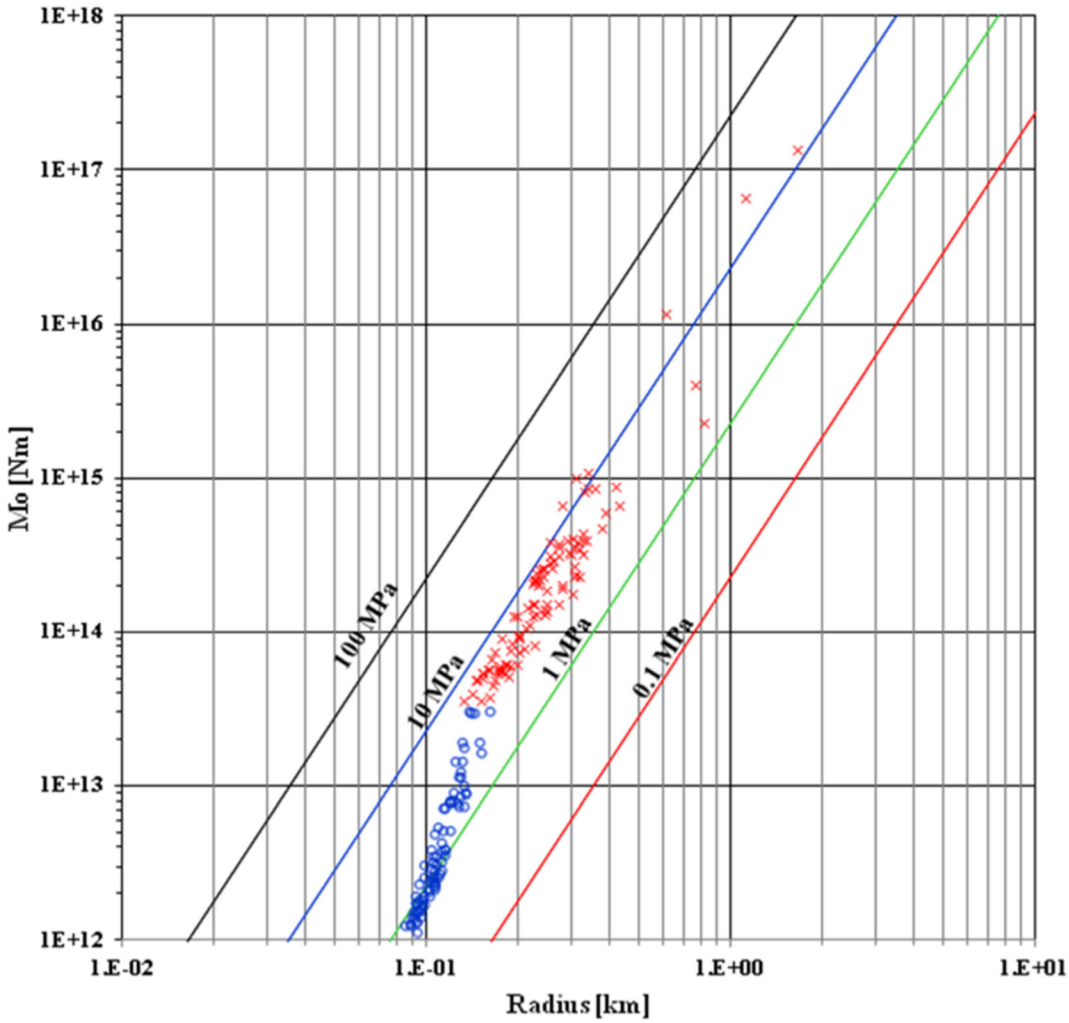


**Fig. 7** The scaling relationship between seismic moments and source radius. The solid lines represent the constant stress drops in the range of 0.1 to 100 MPa

and McNutt (1997) to be triggered due to adjacent high-frequency events among the 1989 earthquake swarm near Long Valley in California.

The averaged $V_P/V_S$ ratio of 1.76 was deduced from the receiver functions in the crust beneath the Arabian Shield (Sandvol et al. 1998; Al-Damegh et al. 2005). Using the H-κ stacking analyses, Tang et al. (2016) inferred $V_P/V_S$ ratios ranging from $1.61 \pm 0.03$ to $2.03 \pm 0.04$. In this study, the $V_P/V_S$ characteristics are presently estimated using a modified WADATI method depending on the differential travel times between P and S phases recording by a pair of corresponding stations. The calculated $V_P/V_S$ ratios are relatively high, which is typical for volcanic and magmatic active regions and seem to be constant for different areas (Nakajima et al. 2001; Ojeda and Havskov 2001; Moretti et al. 2009; Jo and Hong 2013). However, temporal variations during a seismic activity should be considered. The present results reveal variations in the $V_P/V_S$ ratios, within the upper crust of the earthquake source zone, of $1.7 \pm 0.003$ and $1.72 \pm 0.002$ before and after the HL seismic activity, characterizing different processes that are inconsistent with the suggested scenario that magma flows were triggered by the main rupture. At the early stage of the HL activity, the low $V_P/V_S$ ratio may be attributed to gas emission or hypocenters located in the region characterized by swarm activity. The measurements of the apparent velocities for P and S waves reveal a decrease in both $V_P$ and $V_S$. Abdelfattah et al. (2017) characterized this stage as a

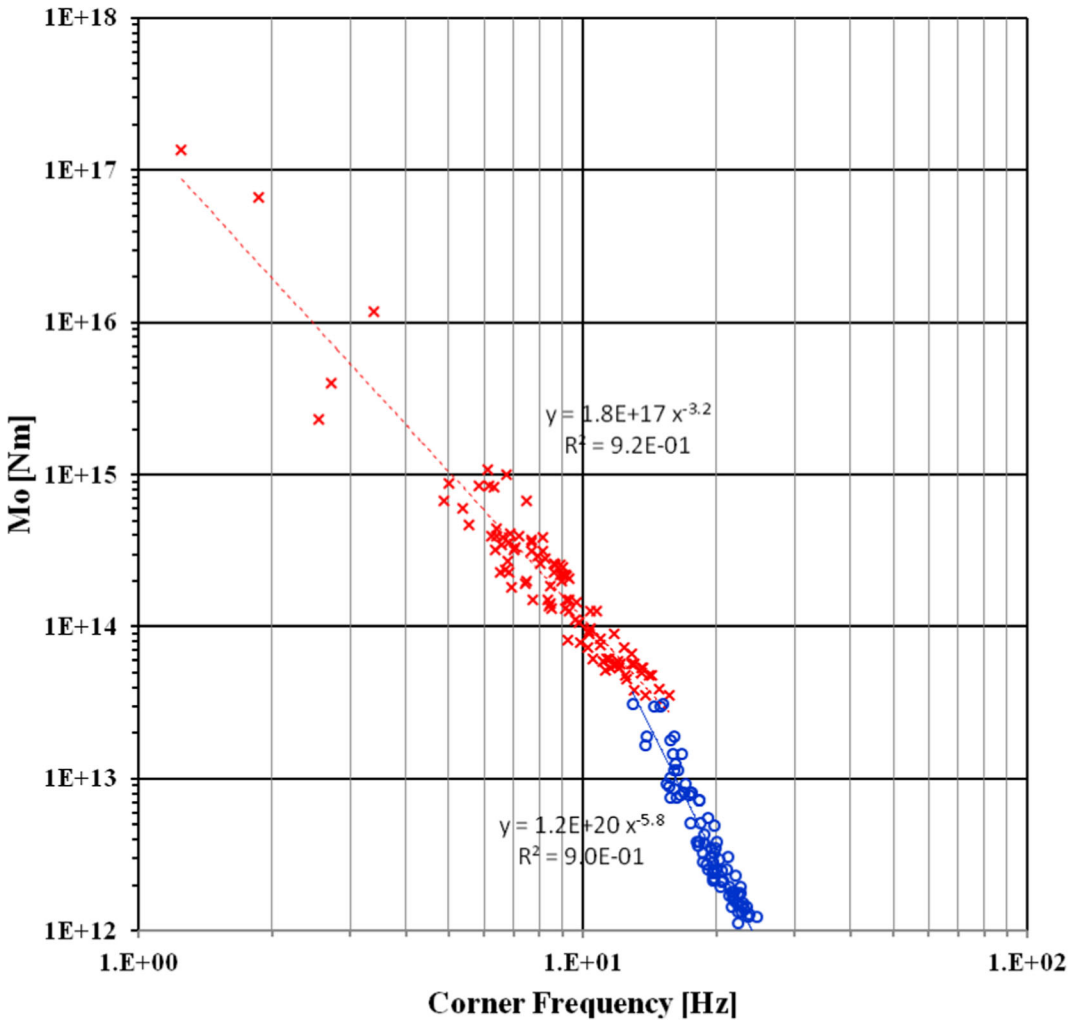


**Fig. 8** The scaling relationship between seismic moments and corner frequencies for the early stage seismic activity (red crosses) and the decay stage seismic activity (open blue circles)

swarm activity that is consistent with the high attenuation zone depicted by Sycher et al. (2017), which support the witnesses of gas emissions in the HL region that reported to the Saudi Geological Survey. Similar changes in the $V_P/V_S$ ratio were observed for the foreshock sequence of Sept. 16, 1997 Umbria-Marche earthquakes (Ripepe et al. 2000) and for the Efpalio earthquake sequence, western Gulf of Corinth, Greece (Giannopoulos et al. 2015). On the other hand, the typical value of $V_P/V_S$ ratio has to be attributed to the non-swarm activity (Abdelfattah et al. 2017) that released after the largest-sized event among the seismic activity due to the stress relaxations.

An interesting result is represented by the deviation of the derived stress drops from constant stress drop models. The source scaling relationships indicate a significant deviation from a homogeneous source model with a constant stress drop, implying that the seismic activity among the early stage was probably emplaced by an upward moving of magmatic dike intrusion that was finally stopped by hardened areas of earlier intrusions in the upper crust. It is obvious (Figure 7) that the events in the early stage are generally characterized by higher stress drops than the events in the decay stage; supporting the suggestion of dike intrusion at the early stage of the analyzed seismic activity (Abdelfattah et al. 2017).

The spatial distribution of inferred stress drops shows that the most part of the stress around the fault zone was released by the early stage activity and that the residual

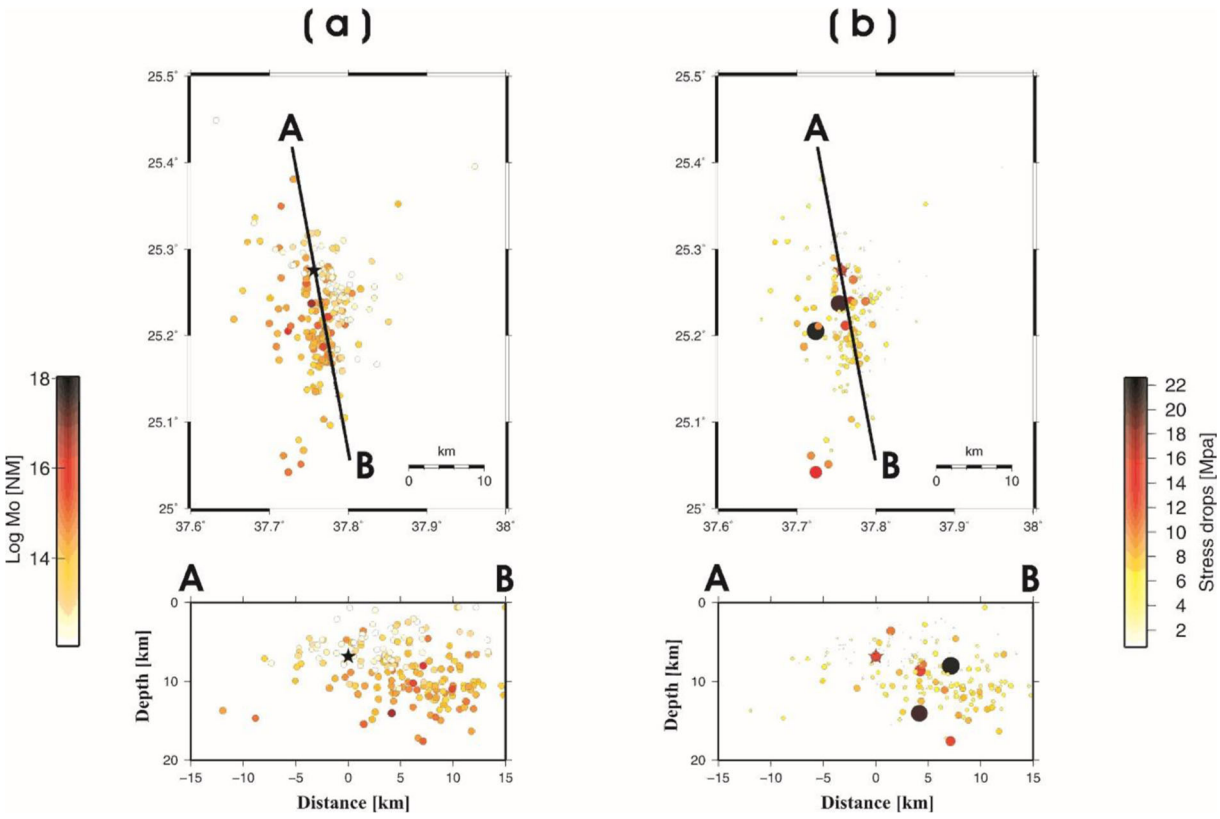


**Fig. 9** The graph showing the epicenter and hypocenter distributions with color consistent with **a** seismic moments and **b** stress drops

stress was released by the decay stage activity. The ambient stress field and previously emplaced dikes in the region may represent strong barriers to the upward movement of magma; thus, the early stage activity may be caused by the upward movement associated with the dike intrusion from 18 km until to a depth of about 7 km where it is stopped by strong materials. This would allow the stress to be accumulated and released in the Mw 5.4 event followed by further seismic activity spread in the fault zone. It is worth stressing that the *b* value obtained by Abdelfattah et al. (2017) reveals that an area of high *b* values coincides with the decay stage activity located southeast of the largest event, while an area of low *b* values coincides with the area of early stage activity and therefore with the area of the HF events.

The results obtained from the present study can be interpreted as a coupling of the volcano- and tectonic earthquake activity. The absence of magmatic eruptions might suggest another geodynamic process: the early stage of seismic activity that related to the emplacement of the dike intrusion; the expansion of dike was stopped in the largest shock area, presumably enriched by magmatic materials in the upper crust from the earlier eruptions. A number of previous studies suggest a dike intrusion associated with magma driven rifting (Baer and Hamiel 2010; Pallister et al. 2010; Mukhopadhyay et al. 2012) or solidified magma of repeated intrusions (Hansen et al. 2013), or an upward migration of partially molten magma source that is not sufficiently strong to initiate eruption (Koulakov et al. 2014, 2015). It is noteworthy that the tomographic inversion imaged the three-dimensional structure in the dislocation zone depends on ray paths of take-off angles greater than 95°, showing a low resolution over the focal zone deeper than 10 km approximately. Moreover, the events among the seismic activity were identified by Pallister et al. (2010) as a volcano-tectonic earthquake type. The low-frequency events were not explicitly observed in the present analysis using recordings from the nearby seismic stations, (only high- and mixed-frequency characteristics were identified). For collocated earthquakes of similar source-to-receiver paths, dissimilarities of frequency contents may attribute to different source

characteristics rather than a propagation effect. The events of higher corner frequencies, of about 20 Hz, imply high and quasi-static stress drops (Abdelfattah et al., 2014). The mechanism of quasi-static stress is suggested for the regions in which no high-stress drops are expected where those ones are characterized by high heat flow, water saturation, numerous cracking, rigid basaltic rocks, and tectonic crustal extension. This mechanism was suggested by Brune et al. 1986 for the Victoria 1978 earthquake swarm.

## 3 Conclusions

In this study, we investigated 218 seismic events, among the HL seismic activity, by means of the spatiotemporal distribution of hypocenters, calculation of $V_P/V_S$ ratios, spectral characteristics of the recorded signals, and estimations of stress drop and source dimensions.

The hypocenters show an upward migration during the early stage activity, starting at a depth of 18 km, whereas the decay stage activity seems to be concentrated in the upper parts of the crust. The calculated $V_P/V_S$ ratios are relatively high which is typical for volcanic and magmatic active regions and seem to be constant for tectonic ones, low to typical $V_P/V_S$ ratios of $1.7 \pm 0.003$ and $1.72 \pm 0.002$ were obtained before and after the largest shock, support the witnesses of gas emissions before the release of the HL largest shock. The analysis of spectrograms exhibited 3 groups; events with only high-frequency content that may be associated with the tectonic process, events with significant low-frequency content that may be associated with the magmatic process, and mixed-events. The results imply important insights on the path propagation between sources and receivers indicating that magmatic materials might be incubated in the upper crust. One of the interesting results is the deviation of the derived stress drops from constant stress drop models. Moreover, the early stage activity is in general characterized by stress drops than higher than the decay stage activity; supporting the assumption of dike intrusion.

Based on the aforementioned observations, we suggest a scenario for the development of the analyzed seismic activity: the early stage of the activity was probably triggered by an upward movement of a magmatic intrusion that might be associated with gas emissions. The intrusion was finally blocked by cooled and hardened areas of earlier intrusions in the upper crust; explaining the absence of magmatic eruptions at the surface. However, stress accumulation continued and was eventually released by the larger-sized event. Owing to the stress relaxation, the activity was decayed with different spectral characteristics and depth distribution.

**Acknowledgments** We are grateful to the Saudi Geological Survey (SGS) for providing the broadband seismic data. The authors would like to extend their sincere appreciation to the Deanship of Scientific Research at King Saud University for funding this Research group no. (RG-1437-010). Generic Mapping Tools developed by Wessel and Smith (1998) was used for most data mapping.

## References

Abdelfattah AK, AlAmri A, Fnais M, Abdelrahman K (2014) Estimation of source parameters and attenuation using digital waveforms of Al-Ays 2009 earthquake, Saudi Arabia. Arab J Geosci 7(8):3325–3337

Abdelfattah AK, Morgen S, Mukhopahyay M (2017) Mapping b-value for 2009 Harrat Lunayyir earthquake swarm, western Saudi Arabia and Coulomb stress for its mainshock. JVGR 330:14–23

Aki K, Richard G (1980) Quantitative seismology: theory and methods. W. H. Freeman, New York

Al-Amri A, Fnais M (2009) Seismo-volcanic investigation of 2009 earthquake swarms at Harrat Lunayyir (Ash Shaqah), Western Saudi Arabia. IntJ Earth Sci Eng India

Al-Damegh K, Sandvol E, Barazangi M (2005) Crustal structure of the Arabian plate: new constraints from the analysis of teleseismic receiver functions. Earth Planet Sci Lett 231:177–196

Aldamegh K, Hussein H, Al-Arifi N, Moustafa S, Moustafa M (2010) Focal mechanism of Badr earthquake, Saudi Arabia of August 27,2009. Arab J Geosci 5(4):599-606

Baer G, Hamiel Y (2010) Form and growth of an embryonic continental rift: InSAR observations and modelling of the 2009 western Arabia rifting episode. Geophys J Int 182(1): 155–167

Borok VK (1959) On estimation of the displacement in an earthquake source and of source dimensions. Ann Geophys 12(2): 205–214

Brown GF (1972) Tectonic map of the Arabian Peninsula, 1:4,000, 000. Kingdom of Saudi Arabia, Ministry of Petroleum and Mineral Resources

Brune JN (1970) Tectonic stress and the spectra of seismic shear waves from earthquakes. J Geophys Res 75(26):4997–5009

Brune JN (1971) Seismic sources, fault plane studies and tectonics. EOS Tras AUG 52:187–187

Brune JN, Fletcher J, Vernon F, Haar L, Hanks T, Berger J (1986) Low stress-drop earthquakes in the light of new data from the Anza, California telemetered digital array. Am Geophys Monogr37:237–245

Camp VE, Hooper PR, Roobol MJ, White DL (1987) The Madinah eruption, Saudi Arabia: magma mixing and

simultaneous extrusion of three basaltic chemical types. Bull Volcanol 49(2):489–508

Chatelain J (1978) Étude fine de la sismicité en zone de collision continentale à l'aide d'un réseau de stations portables: la région HinduKush–Pamir, Ph.D. thesis, Université Paul Sabatier, Toulouse

Chatterjee SN, Pitt AM, Iyer HM (1985) Vp/Vs ratios in the Yellowstone national park region, Wyoming. JVGR 26: 213–230

Chouet BA (1996) Long-period volcano seismicity: its source and use in eruption forecasting. Nature 380(6572):309–316

Craig TJ, Jackson JA, Priestley K, McKenzie D (2011) Earthquake distribution patterns in Africa: their relationship to variations in lithospheric and geological structure, and their rheological implications. GJI 185(1):403–434

Cramer CH, McNutt SR (1997) Spectral analysis of earthquakes in the 1989 Mammoth Mountain swarm near Long Valley, California. Bull Seismol Soc Am 87(6):1454–1462

de Lorenzo S, Zollo A, Zito G (2010) Source, attenuation, and site parameters of the 1997 Umbria - Marche seismic sequence from the inversion of P wave spectra: a comparison between constant QP and frequency-dependent QP models. J Geophys Res 115:B09306. https://doi.org/10.1029/2009JB007004

Daradich A, Mitrovica JX, Pysklywec RN, Willett SD, Forte AM (2003) Mantle flow, dynamic topography, and rift-flank uplift of Arabia. Geology 31(10):901–904

Dawson P, Chouet B (2014) Characterization of very-long-period seismicity accompanying summit activity at Kilauea volcano, Hawai'i: 2007–2013. JVGR 278–279:59–85

Domański B (2007) Source parameters of the 2004 Kaliningrad earthquakes. Acta Geophysica 55(3):267–287

Duda S, Kaiser D (1989) Spectral magnitudes, magnitude spectra and earthquake quantification; the stability issue of the corner period and of the maximum magnitude for a given earthquake. Tectonophysics 166(1–3):205215–211219

Duda S, Xu S (1988) Broad-band seismograms, band-pass seismograms, and spectral magnitudes for a selection of 1978-1983 explosions–comparison with worldwide earthquakes. Inst Geophys Univ Hamburg

El-Isa Z, Shanti A (1989) Seismicity and tectonics of the Red Sea and western Arabia. Geophys J Int 97(3):449–457

Eshelby JD (1957) The determination of the elastic field of an ellipsoidal inclusion, and related problems. Proc R Soc Lond A

Giannopoulos D, Sokos E, Konstantinou KI, Tselentis G (2015) Shear wave splitting and *VP*/*VS* variations before and after the Efpalio earthquake sequence, western Gulf of Corinth, Greece. GJI 200:1436–1448

Grandin R, SOcquet A, Binet R, Klinger Y, Jacques E, de Chabalier J-B, King GCP, Lasserre C, Tait S, Tapponnier P, Delorme A, Pinzuti P (2009) September 2005 Manda Hararo-Dabbahu rifting event, Afar (Ethiopia): constraints provided by geodetic data. J Geophys Res Solid Earth 114(B8)

Gritto R, Jarpe SP (2014) Temporal variations of Vp/Vs-ratio at the geysers geothermal field, USA. Geothermics 52:112–119

Hansen SE, Deshon HR, Moore-Driskell MM, AlAmri AM (2013) Investigating the P wave velocity structure beneath Harrat Lunayyir, northwestern Saudi Arabia, using double-difference tomography and earthquakes from the 2009 seismic swarm. J Geophys Res Solid Earth 118(9):4814–4826

Hill DP (1977) A model for earthquake swarms. J Geophys Res 82(8):1347–1352

Hanks T, Wyss M (1972) The use of body-wave spectra in the determination of seismic-source parameters. BSSA 62:561–589

Ibs-von Seht M, Plenefisch T, Klinge K (2008) Earthquake swarms in continental rifts—a comparison of selected cases in America, Africa and Europe. Tectonophysics 452(1–4): 66–77

Jo E, Hong T-K (2013) V P/V S ratios in the upper crust of the southern Korean Peninsula and their correlations with seismic and geophysical properties. J Asian Earth Sci 66:204–214

Johnson PR (2006) Explanatory notes to the map of Proterozoic geology of Western Saudi Arabia. Technical Report SGS-Tr-2006-4

Kaviris G, Millas C, Spingos L, Kapetanidis V, Fountoulakis I, Papadimitriou P, Voulgaris N, Makropoulos K (2018) Observations of shear-wave splitting parameters in the Western Gulf of Corinth focusing on the 2014 Mw=5.0 earthquake. PEPI 282:60–76

Kiratzi A, Soks E, Ganas A, Tselentis A, Benetatos C, Roumelioti Z, Serpetsidaki A, Andriopoulos G, Galanis O, Petrou P (2008) The April 2007 earthquake swarm near Lake Trichonis and implications for active tectonics in western Greece. Tectonophysics 452(1):51–65

Kisslinger C, Engdahl E (1973) The interpretation of the Wadati diagram with relaxed assumptions. BSSA 63(5):1723–1736

Koulakov I, ElKhrepy S, Al-Arifi N, Sychev I, Kuznetsov P (2014) Evidence of magma activation beneath the Harrat Lunayyir basaltic field (Saudi Arabia) from attenuation tomography. Solid Earth 5(2):873–882

Koulakov I, ElKhrepy S, Al-Arifi N, Kuznetsov P, Kasatkina E (2015) Structural cause of a missed eruption in the Harrat Lunayyir basaltic field (Saudi Arabia) in 2009. Geology 43(5):395–398

Levshin AL, Pisarenko VF, Pogrebinsky GA (1972) Frequency-time analysis of oscillations. Annales de Geophysique, Editions CNRS 20/22 Rue ST. Amand, 75015 Paris, France

Londoño JM (2010) Activity and *VP*/*VS* ratio of volcano-tectonic seismic swarm zones at Nevado del Ruiz Volcano, Colombia. Earth Sci Res J 14:111–124

Lopes AEV, Assumpcão M (2011) Genetic algorithm inversion of the average 1D crustal structure using local and regional earthquakes. Comput Geosci 37:1372–1380

Maggi C, Frepoli A, Cimini GB, Console R, Chiappini M (2009) Recent seismicity and crustal stress field in the Lucanian Apennines and surrounding areas (Southern Italy): Seismotectonic implications. Tectonophysics 463:130–144

McNutt SR (2005) Volcanic seismology. Annu Rev Earth Planet Sci 32:461–491

Moretti M, De Gori P, Chiarabba C (2009) Earthquake relocation and three-dimensional V p and V p/V s models along the low angle Alto Tiberina Fault (Central Italy): evidence for fluid overpressure. Geophys J Int 176(3):833–846

Mukhopadhyay B, Mogren S, Mukhopadhyay M, Dasgupta S (2012) Incipient status of dyke intrusion in top crust – evidences from the Al-Ays 2009 earthquake swarm, Harrat Lunayyir, SW Saudi Arabia. Geomat Nat Haz Risk:1–19

Nakajima J, Matsuzawa T, Hasegawa A, Zhao D (2001) Three-dimensional structure of Vp, Vs, and Vp/Vs beneath northeastern Japan: implications for arc magmatism and fluids. JGR Solid Earth 106(B10):21843–21857

Neuberg JW, Tuffen H, Collier L, Green D, Powell T, Dingwell D (2006) The trigger mechanism of low-frequency earthquakes on Montserrat. JVGR 153(1):37–50

Nobile A, Pagli C, Keir D, Wright TJ, Ayele A, Ruch J, Acocella V (2012) Dike-fault interaction during the 2004 Dallol intrusion at the northern edge of the Erta Ale Ridge (Afar, Ethiopia). GRL 39(19)

Ojeda A, Havskov J (2001) Crustal structure and local seismicity in Colombia. J Seismol 5(4):575–593

Pallister JS, Mccausland WA, Johnson S, Lu Z, Zahran HM, Hadidy SE, Aburukbah A, Stewart ICF, Lundgren PR, White RA, Moufti MRH (2010) Broad accommodation of rift-related extension recorded by dyke intrusion in Saudi Arabia. Nat Geosci 3:705–712

Prieto G, Shearer PM, Vernon FL, Kilb D (2004) Earthquake source scaling and self-similarity estimation from stacking P and S spectra. J Geophys Res 109:1–13 B08310

Pedersen R., Sigmundsson F, Einarsson P (2007) Controlling factors on earthquake swarms associated with magmatic intrusions: Constraints from Iceland. JVGR 162:73-80

Ripepe M, Piccinini D, Chiaraluce L (2000) Foreshock sequence of the September 26th, 1997 Umbria-Marche earthquakes. JOS 4:387–399

Rodgers A, Walter W, Mellors R, Al-Amri A, Zhang Y (1999) Lithospheric structure of the Arabian Shield and Platform from complete regional waveform modelling and surface wave group velocities. Geophys J Int 138:871–878

Sandvol E, Seber D, Barazangi M, Vernon F, Mellors R, Al-Amri A (1998) Lithospheric seismic velocity discontinuities beneath the Arabian Shield. GRL 25:2873–2876

Saul J (1995) A computer program (nfilter) for spectral seismogram calculation. Institute of Geophysics, Hamburg University, Hamburg

Sychev I, Koulakov I, ElKhrepy S, Al-Arifi N (2017) Pathways of volatile migration in the crust beneath Harrat Lunayyir (Saudi Arabia) during the unrest in 2009 revealed by attenuation tomography. JVGR 330:1–13

Tang Z, Julià J, Zahran H, Mai PM (2016) The lithospheric shear-wave velocity structure of Saudi Arabia: young volcanism in an old shield. Tectonophysics 680:8–27

Tuffen H, Dingwell D (2005) Fault textures in volcanic conduits: evidence for seismic trigger mechanisms during silicic eruptions. Bull Volcanol 67:370–387

Ukawa M, Fukao Y (1981) Poisson's ratios on the upper and lower crust and the sub-Moho mantle beneath central Honshu, Japan. Tectonophysics 77:233–256

Wessel P, Smith WH (1998) New, improved version of Generic Mapping Tools released. EOS Trans Am Geophys Union 79: 579–579

Wilde-Piorko M, Duda S, Grad M (2011) Frequency analysis of the 2004 Sumatra–Andaman earthquake using spectral seismograms. Acta Geophysica 59(3):483–501. https://doi.org/10.2478/s11600-011-0010-8

Wright TJ, Ebinger C, Biggs J, Ayele A, Yirgu G, Keir D, Stork A (2006) Magma-maintained rift segmentation at continental rupture in the 2005 Afar dyking episode. Nature 442:291–294

Zobin VM, Al-Amri AM, Fnais M (2013) Seismicity associated with active, new-born, and re-awakening basaltic volcanoes: case review and the possible scenarios for the Harraat volcanic provinces, Saudi Arabia. Arab J Geosci 6(2):529–541